Astron. Astrophys. 329, 233–242 (1998)

ASTRONOMY
AND
ASTROPHYSICS

H II and hot dust emission around young massive stars in G9.62+0.19

Leonardo Testi[1,2], **Marcello Felli**[3], **Paolo Persi**[4], **and Miguel Roth**[5]

[1] Dipartimento di Astronomia e Scienza dello Spazio, Università degli Studi di Firenze, Largo E. Fermi 5, I-50125 Firenze, Italy
[2] California Institute of Technology, Division of Physics, Math and Astronomy, 105-24, Pasadena, CA 91125, USA
[3] Osservatorio Astrofisico di Arcetri, Largo E. Fermi 5, I-50125 Firenze, Italy
[4] Istituto di Astrofisica Spaziale, C.N.R., C.P. 67, I-00044 Frascati, Italy
[5] Las Campanas Observatory, Casilla 601, La Serena, Chile

Received 21 May 1997 / Accepted 7 August 1997

Abstract. In this paper we present new near infrared (NIR) observations (J, H, and K broadbands), of the G9.62 + 0.19 star forming complex.

Comparison of our observations with similar resolution centimetric continuum, millimeter continuum and molecular emission show that the mm continuum source F, not detected in the cm wavelength free-free radio continuum and associated with a high density molecular peak, is detected at 2.2 μm, while the ultracompact HII region D, one of the youngest of the HII regions in the complex, is not detected in the near infrared.

We propose a simple model that explains why, in the first stages of evolution of a young massive star, the source may be observable at K but not in the cm radio continuum. When the size of the UC HII region is $\ll 10^{-3}$ pc the hot dust present around the YSO strongly emits at K band, but the radio emission will be strongly self-absorbed. At later stages, when the size of the UC HII becomes greater than $\gtrsim 10^{-3}$ pc, the dust temperature goes down and the K band dust emission strongly decreases; at the same time the cm radio continuum becomes detectable. As the UCHII expands the extinction drops and the K band emission rises again due to the stellar and ionized gas free-free and free-bound emission.

We propose an evolutionary sequence of the different sites of star formation in the complex, based on the radio continuum–infrared morphology and on the association with H_2O masers.

Key words: ISM: H II regions; molecules; jets and outflows – star formation – infrared: ISM: continuum – ISM: G9.62+0.19

1. Introduction

Although originally associated with advanced stages of massive star formation (such as diffuse HII regions), H_2O masers are now believed to be associated with the earliest phases of massive star formation. Several pieces of evidence (Palla et al. 1993; Codella et al. 1994) suggest that the masers are associated with massive stars that have not even had the time to develop an ultra compact (UC) HII region. High resolution radio continuum and maser line observations (Forster & Caswell 1989; Tofani et al. 1995; Hofner & Churchwell 1996) showed that the majority of the H_2O maser spots, although generically associated with high mass star forming regions (i.e. HII regions), are not closely related to compact radio continuum sources, suggesting that they must have a close-by exciting source, independent from the ones that power more diffuse HII regions in the same complex. On the other hand, the masers are always associated with dense hot molecular cores and compact mm wavelength and far infrared continuum sources (Cesaroni et al. 1991; 1994, hereafter CCHWK; Codella et al. 1997; Jenness et al. 1996; Cesaroni et al. 1997), indicating that the powering source for the masing gas should be a Young Stellar Object (YSO) still deeply embedded in its parental molecular clump.

To unveil the short wavelength tail of the spectral energy distribution (SED) of the sources associated with the masers, and to better constrain their age and evolutionary status, we have undertaken a survey at near infrared wavelengths ($1 - 2.4$ μm) of galactic H_2O masers sources. In a preliminary sub-sample (Testi et al. 1994) observed with moderate sensitivity (although the survey is much deeper and with higher resolution than any one done so far), we were able to find a NIR source reliably associated with the maser source in almost 90% of the objects. The infrared characteristics of these sources, namely a very large infrared excess (H–K)> 2, suggested that they are YSOs deeply embedded in molecular cores. In particular, the NIR colours of the objects could not be explained in terms of extincted stellar photospheres, but a large fraction of the observed radiation had to be produced by dusty envelopes heated to high temperatures (up to 1000 K) by the YSO radiation field. Given the expected mass of the objects and the lack of radio continuum emission the sources were suggested to be in a pre-UC HII region phase.

Send offprint requests to: Testi, Caltech, (lt@astro.caltech.edu)

A few sources analysed in greater detail (Hunter et al. 1995; Palla et al. 1995; Persi et al. 1996; Felli et al. 1997; Cesaroni et al. 1997) confirmed this view, and emphasized the power of coordinated multi-wavelength observations with high resolution and sensitivity.

In this paper we will focus our attention on the star forming complex G9.62 + 0.19. This is quite an interesting case, since a cluster of HII regions placed at a distance of 5.7 kpc (Hofner et al. 1994) in different evolutionary phases (i.e. with different sizes and mean densities) is present.

Radio continuum observations made at several wavelengths with different resolutions showed the presence of five components, labelled from A to E (Garay et al. 1993; Kurtz, Churchwell & Wood 1994; CCHWK). From west to east: component A is a diffuse and extended ($\sim$ 0.5′ diameter) HII region, with mean density 2×10^2 cm^{-3}; component B is a less extended ($\lesssim$ 0.3′, mean density 2×10^3 cm^{-3}) cometary (or blister shaped) HII region, with the tail toward the south-west. Toward the north-east there are three compact radio continuum components C, D, and E, classified as UC HII regions. The radio components detected by CCHWK are labelled in Fig. 2 and 3. Note that component A lies outside the area shown in the figures (see Fig. 3 of Garay et al. 1993).

Low resolution single dish molecular observations of Cesaroni et al. (1991) and Cesaroni, Walmsley & Churchwell (1992), revealed a molecular core associated with the cluster, but could only rule out the association of the hot molecular material with radio continuum component A (the more evolved), without being able to indicate which of the other components was likely to be associated with the molecular peak.

The region shows maser emission of several interstellar high-excitation molecules. High resolution VLA observations of the OH (Forster & Caswell 1989; Forster 1993), CH_3OH (Norris et al. 1993), H_2O (Forster & Caswell 1989; Forster 1993; Hofner & Churchwell 1996) and NH_3(5,5) (Hofner et al. 1994) masers showed that the maser spots are concentrated in a filamentary structure extending from component D to E. In particular the H_2O masers are found close to components D, E, and F. The comparison of the number, positions and intensities of the spots detected by Forster & Caswell (1989) and those detected by Hofner & Churchwell (1996) show some distinct changes which reflect the variability of the maser activity. Here we will use the observations of Hofner & Churchwell (1996) because they are more sensitive and with higher resolution.

Interferometric observations of the NH_3 inversion lines (CCHWK, Hofner et al. 1994) showed that there is a molecular clump associated with the maser activity, close to component D, but a few seconds of arc to the north of the radio continuum region. A fainter ammonia clump was found associated with component E.

Interferometric NH_3(4,4) (CCHWK) and millimeter continuum and molecular line observations (Hofner et al. 1996) revealed the presence of a sixth component (F) $\sim$ 4″ north of component D which does not have detectable centimeter wavelength radio continuum emission, but it is the strongest source in the field at mm continuum and in the NH_3(4,4) and CH_3CN(J=6−5) lines. The strongest H_2O maser spots are located between component F and component D. The $C^{18}O(1-0)$ interferometric spectra taken at the position of component F show a compact molecular component with broad wings, with asymmetric structure, which was interpreted as a localized bipolar molecular outflow associated with component F (Hofner et al. 1996). From their mm continuum and molecular line data Hofner et al. concluded that component F is the youngest object in the region and that it is probably a high mass star still in the accretion phase.

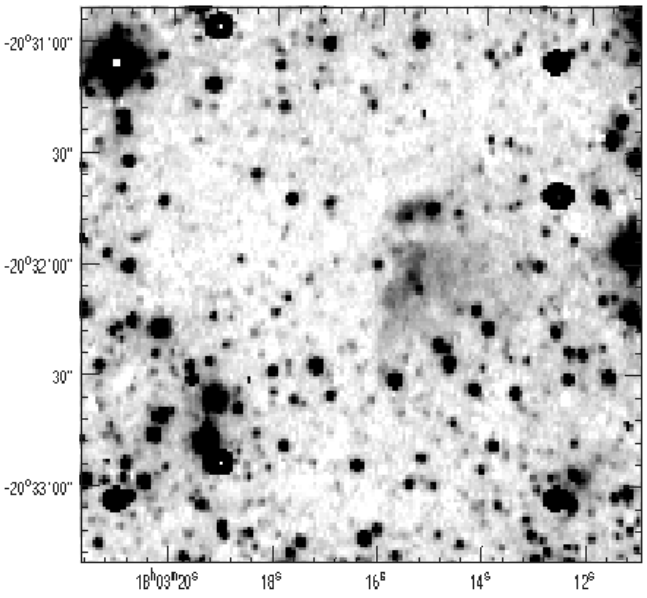

Fig. 1. K-band greyscale image of the $\sim 2.5' \times 2.5'$ observed region. North is at top and east to the left.

In this paper we present J,H, and K near infrared images of the whole star forming region. The observations are described in Sect. 2. The results are presented in Sect. 3. In Sect. 4 we discuss the evolutionary status of the sources in the region, focusing our attention on the two sources F and D, and presenting a simple model that can explain the occurrence of NIR and radio emission during the evolution of a massive star. Finally in Sect. 5 we summarize the main conclusions of this work.

2. Observations

2.1. Near infrared observations

The near infrared images were obtained in the framework of an extensive project of infrared observations of galactic maser sources (Testi et al. 1994; 1995; 1997). Broad band near infrared observations were taken on June 4^{th} 1992 with a NICMOS3 (256×256 HgCdTd pixels) camera (Persson et al. 1992) mounted at the 1 m telescope of the Las Campanas Observatory. The scale on the detector was 0.92″/pix. The source was observed at J, H and K (1.25, 1.65 and 2.2 μm respectively) using a dithering technique: five partially overlapping frames were

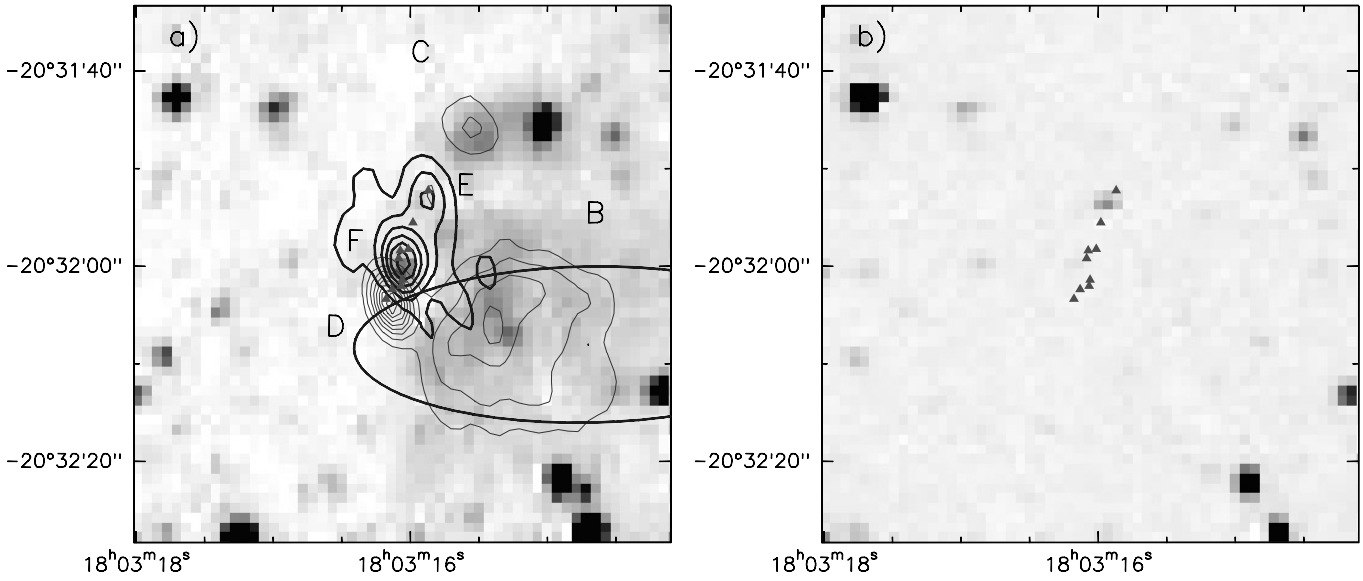

Fig. 2. a K-band greyscale image of the $\sim 1' \times 1'$ region centered on the H_2O maser position. **b** J-band greyscale of the same region. In both images the H_2O maser spots detected by Hofner & Churchwell 1996 are indicated with filled triangles (symbols are larger than the position uncertainties). On the K-band image the VLA D-array radio continuum (thin contours) and $NH_3(4,4)$ emission (thick contours) observed by CCHWK are reported; the cm and mm components B, C, D, E, and F are labelled; component A lies to the west (outside the plotted area), see Fig. 3 of Garay et al. (1993). The contour values are: from 10 to 90 by 10 mJy/beam and from 10 to 70 by 10 mJy/beam, for the continuum and line emission respectively. The large ellipse is the error box of IRAS18032 − 2032. Coordinates are at B1950.

taken in each band; the flat field image was calculated by clipping and median averaging the five frames taken in each band. After flat fielding, the images were registered and mosaiced together in order to increase the signal to noise ratio in the common area (centered on the nominal H_2O maser position). All the data reduction and analysis was performed using the IRAF[1] and ARNICA[2] (Hunt et al. 1994) software packages. The K-band image of the observed region is shown in Fig. 1.

Photometric calibration was achieved by observing some of the UKIRT faint standards (Casali & Hawardeen 1992). The photometric accuracy is estimated to be $\sim$ 5%. The limiting magnitudes in the overlapping region (3σ in 4 arcsec aperture) are: 16.3, 15.4 and 14.4, at J, H and K respectively.

Astrometric calibration was performed using a set of optical stars extracted from the Digitized Sky Survey, made available by the Space Telescope Science Institute. We estimate the calibration accuracy to be better than 1 arcsec (see Testi 1993, for a complete description of the astrometric calibration procedure).

2.2. H_2O maser observations

The water maser emission in G9.62+0.19 has been observed in four different epochs (3/87, 6/87, 1/91, 1/94) with the 32 m Medicina[3] VLBI antenna (observational procedures and instrumental setup are described in Brand et al. 1994). The observations are part of the Arcetri H_2O masers variability monitoring program.

3. Results

In Fig. 2a the K band image of a region $1' \times 1'$ wide centered on the maser position is shown. Fig. 2b shows the J band image of the same region. In both figures the maser spots detected by Hofner & Churchwell (1996) are also shown. It can be clearly seen that the masers are well separated from the diffuse K-band emission (and the diffuse radio continuum emission). All the maser spots lie towards the north-east of the infrared diffuse emission, approximately at the position of the components D, E, and F.

As also found in other regions (see e.g. Testi et al. 1994), the IRAS source is not coincident with the H_2O maser and compact radio continuum components, but is associated with the extended K-band and radio continuum emission. Consequently the IRAS fluxes are indicative of the global infrared emission of the area and the luminosity of $4.3 \times 10^5\,L_\odot$ given by CCHWK refers to all the sources in the area.

The comparison between our near infrared images and the radio continuum maps of Kurtz et al. (1994) and CCHWK show that at 2.2 μm we detect emission from the radio continuum sources B, C, and E, but not from A and D. Radio source A is

[1] IRAF is made available to the astronomical community by the National Optical Astronomy Observatories, which are operated by AURA, Inc., under contract with the U.S. National Science Foundation

[2] ARNICA can be obtained from the Osservatorio Astrofisico di Arcetri at `ftp://150.217.20.1/pub/arnica/`

[3] The Medicina telescopes are operated by the Istituto di Radioastronomia (CNR), Bologna, Italy.

probably so diffuse that it has a surface brightness at K-band too low to be detected. More difficult to explain is the lack of K-band emission from the UC HII region D, which is associated with a star of spectral type earlier than O9.5 (CCHWK). In Fig. 3, the $NH_3(4,4)$ and radio continuum emission are overlaid on the K-band image. From the figure, it can be clearly seen that a NIR source is found coincident with component F, which is defined by the ammonia clump, some of the strongest H_2O maser spots and the mm continuum, but it does not have cm-wavelength radio continuum emission. Component F is detected only at K-band, with upper limits at J and H, indicating that it is heavily extincted and has a large NIR excess.

In Fig. 4 (upper panel) the (J–H,H–K) colour-colour diagram of the near infrared sources detected in a $2.5' \times 2.5'$ area around the maser position is presented. About 12% of the detected NIR sources show infrared excess, and are probably young stellar objects surrounded by hot dust, either in circumstellar disks or envelopes. The NIR sources associated with radio components C, E, and F and the point source inside component B (called NIR–B$\star$ to avoid confusion between diffuse emission and the pointlike "stellar" component) are marked. All the sources show NIR excess, source F being the reddest of the whole field. In Fig. 4 (lower panel) a diagram showing the position of the NIR sources on the sky is also presented. It is worth noting that the infrared excess sources (filled diamonds) are not confined inside a well defined cluster as usually found in similar regions (see e.g. Cesaroni et al. 1997 for the case of IRAS20126+4104 or Persi et al. 1997 for G35.20−1.74).

In Table 1, the observed parameters of the NIR sources associated with the radio and mm continuum components are shown (note that the value of δ for radio continuum source C in Table 4 of CCHWK is incorrect). For each source the first column gives the identifier, the second and third the coordinates at 1950 epoch, and the fourth, fifth and sixth the magnitudes measured in the J, H and K filters, respectively. When no error is reported, and a symbol ">" is indicated, the source has not been detected in that filter, and the quoted magnitude is a lower limit (i.e. the correnspondingflux is an upper limit).

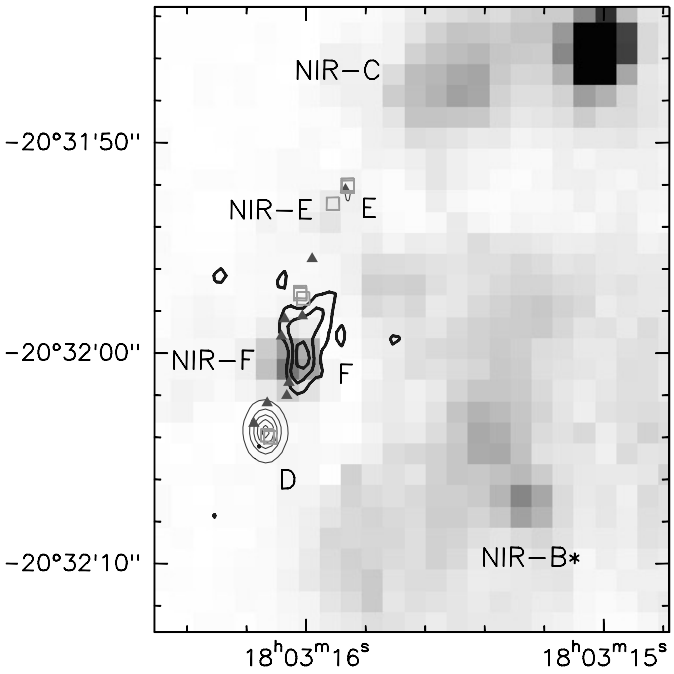

Fig. 3. Greyscale: enlargement of the K-band image of Fig. 2. Contours: VLA C-array radio continuum at 1.3 cm (thin contours) and $NH_3(4,4)$ (thick contours) emission observed by CCHWK. Filled triangles: H_2O maser spots detected by Hofner & Churchwell (1996). Open squares: OH maser spots from Forster (1993). Contour levels are: 10, 30, 50, 70, 90 mJy/beam and 8, 13, 18 mJy/beam, for radio continuum and NH_3(4,4) respectively. The cm and mm components D, E, and F, as well as the NIR sources NIR-B$\star$, NIR-C, NIR-E and NIR-F, are labelled (see text). Coordinates are at B1950.

3.1. Radio components A and B

In the radio continuum both components A and B are diffuse and have an optically thin spectrum. Radio source A is the largest source of the complex. Its surface brightness at K is too low to be detected by these observations. Radio source B has a cometary or blister morphology, with the "tail" directed to the south-west. Component B is detected in the near infrared as a diffuse component, detected only at K, and a point source near to the radio continuum peak (see Table 1). From the radio continuum observations, CCHWK found that the source responsible for the ionization should be an O7.5 zero age main sequence (ZAMS) star. We believe that the point source inside the diffuse K-band emission coincides with the star responsible for the ionization of the HII region. The colours and magnitudes of this source (NIR–B$\star$) are compatible with the magnitudes and colour of an O7.5 star at 5.7 kpc and with an extinction of $A_V \simeq 30$, assuming a Rieke & Lebofsky (1985) extinction law and intrinsic colour and magnitudes from Koornneef (1983) and Schmidt-Kaler (1981). In fact, an O7.5 main sequence star should have (H−K)= −0.05, and $M_H = -4.2$ (we use the magnitude measured in the H-band, instead of that measured at K, because at H the contribution of the infrared excess should be much lower than the photospheric emission), which are consistent with the observations, assuming $A_V \simeq 30$, and the presence of a moderate infrared excess at K.

3.2. Radio component C

At K band, this source is almost pointlike and its colour and magnitude cannot be simply explained as a reddened B0 ZAMS star (required to explain the radio continuum emission). From the NIR colours and magnitudes (see Table 1 and Fig. 4) we expect that a large fraction of the K-band emission is not due to the (reddened) stellar photosphere, but is probably coming from hot circumstellar dust.

3.3. Radio component D

This source is not detected in our near infrared images, hence we can only quote upper limits for its magnitudes ($m_J >$

Table 1. Observed parameters of the NIR sources associated with the cm and mm components

Name	α (1950)	δ (1950)	m_J	m_H	m_K
NIR-B$\star$	18 : 03 : 15.39	-20 : 32 : 05.4	> 16.7	14.7 ± 0.1	12.3 ± 0.05
NIR-C	18 : 03 : 15.49	-20 : 31 : 47.5	> 16.7	14.4 ± 0.1	12.1 ± 0.04
NIR-E	18 : 03 : 15.94	-20 : 31 : 53.6	15.5 ± 0.07	15.0 ± 0.2	14.0 ± 0.2
NIR-F	18 : 03 : 16.15	-20 : 32 : 0.0	> 16.7	> 15.4	12.9 ± 0.08

16.7, $m_H > 15.4$, $m_K > 14.5$). Considering that the ionizing star should be earlier than O9.5 (CCHWK), we derive an extinction toward the source greater than 40 magnitudes in the visual.

3.4. Radio component E

This is the only source detected in all the three NIR broad bands (see. Table 1). The source has a near infrared excess as shown in Fig. 4, and it is probably more evolved than the other sources which are associated with H_2O masers. Assuming a spectral type B1 (required to explain the radio continuum emission, see CCHWK and Hofner et al. 1996) we find that the infrared colours of the source are compatible with those of a ZAMS star extincted by more than 30 magnitudes (in the visible) and with a substantial infrared excess.

3.5. The mm and molecular component F

Taking into account the upper limits in the J and H emission, this is the source with the largest NIR excess in the field (H–K>2.5, see. Fig. 4 and Table 1). This source is close to the strongest H_2O maser source (located midway between this component and component D) and associated with a molecular outflow observed in $C^{18}O$ (1–0) (Hofner et al. 1996). The large infrared excess, the association with the maser source, the presence of a molecular hot core, the mm dust emission, the lack of a radio UC HII region, and the molecular outflow, all point to the conclusion that this is the youngest source of the complex. From the inferred temperature and size of the molecular condensation Hofner et al. 1996 derive an expected luminosity of the central star of $\sim 1.8 \times 10^4$ $L_\odot$ which would correspond to a B0–B0.5 ZAMS star. Assuming that CCHWK do not detect radio continuum emission from component F due to beam dilution, and assuming that the free-free emission is optically thick, one can derive an upper limit on the size of the (expected) HII region embedded inside the molecular clump. We derive a (3σ) upper limit on the radius of 1.5×10^{-2} arcsec, which corrensponds to 4×10^{-4} pc at 5.7 kpc.

4. Discussion

There are several models that fit the far infrared emission of embedded high-mass young stars (see e.g. Natta & Panagia 1976; Churchwell, Wolfire & Wood 1990). However all of these models are focused on the interpretation of the far infrared emission, which originates from the large scale dusty envelope around the star and is dominated by the cooler dust. Accurate modelling of the near infrared emission from young stars has been performed for low and intermediate mass stars (Beckwith et al. 1990; Natta et al. 1993; Calvet, Hartmann & Strom 1997) where no ionizing radiation is present.

Since we are primarily interested in the near infrared emission during the first stages of evolution of high mass stars, we have developed a qualitative evolutionary model focused on hot circumstellar dust to explain the present observational results.

Such a model should be able to explain why source F is observed in K band, but not in the cm radio continuum down to ~ 4 mJy at 22 GHz, while source D is observed in the cm radio continuum but not in the near infrared.

4.1. A simple evolutionary model

We will consider three contributions to the near infrared emission: the stellar photosphere, the free-free and free-bound emission from ionized gas and the hottest layer of the dusty envelope which surrounds the YSO. We will assume a spherically symmetric model, thus neglecting anisotropies introduced by an accretion disk and/or an outflow. Similarly, the contribution of radiation escaping through optically thin paths of the envelope and reflected into the line of sight of the observer will not be considered.

The photospheric emission in the near infrared bands has been estimated using the calibration of Schmidt-Kaler (1981) and Koornneef (1983). The free-free and free-bound ionized gas emission in the NIR has been computed using the emission coefficients of Sibille et al. (1974). The dusty envelope is assumed to emit in the near infrared as a black body with the temperature and size of the hottest dusty layer (the one closest to the star). Such an assumption is valid if only the hottest layers of the dust shell contribute significantly to the NIR emission, while the external colder layers of the large scale dusty molecular cloud provide most of the extinction but negligible NIR emission.

The contribution of each type of emission may change during the evolution of the source. When the extinction is large it is very unlikely that the stellar photosphere and the free-free and free-bound emission from the ionised gas give the main contribution to the observed emission at 2.2 μm, this may be the case for component F. On the other hand, in more evolved cases, such as component B, the pointlike infrared component (NIR-B$\star$) can be easily explained in terms of a stellar photosphere of an early type star surrounded by an optically thin HII region, extincted by optically thick ($A_V \simeq 30$) cold dust.

A young source, which has not even had time to develop an observable UC HII region or if the expansion of the ionized gas is quenched by a strong accretion rate (Walmsley 1995), may still

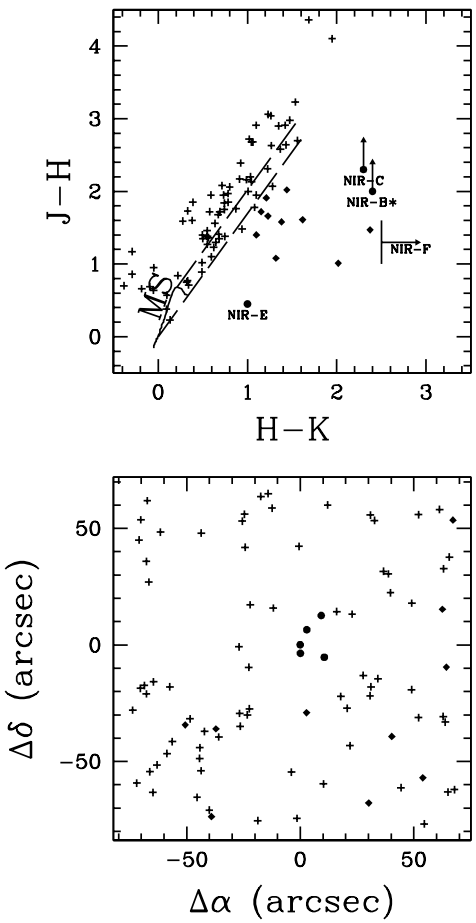

Fig. 4. Upper panel: (J–H,H–K) colour-colour diagram of the near infrared sources detected in a $\sim 2.5' \times 2.5'$ region around the maser position (shown in Fig. 1). The line labelled MS represents the colours of main sequence stars (Koorneef 1983). The two dashed lines define the region in which reddened main sequence stars should lie (assuming Rieke & Lebofsky 1985 interstellar extinction law). Sources with infrared excess are indicated with filled diamonds. Lower panel: positions of the NIR sources plotted in the colour-colour diagram. The offsets are calculated from the position of source NIR-F (see text). Filled diamonds represent infrared excess sources; filled circles represent the positions of sources NIR-B⋆, NIR-C, NIR-E, D and NIR-F.

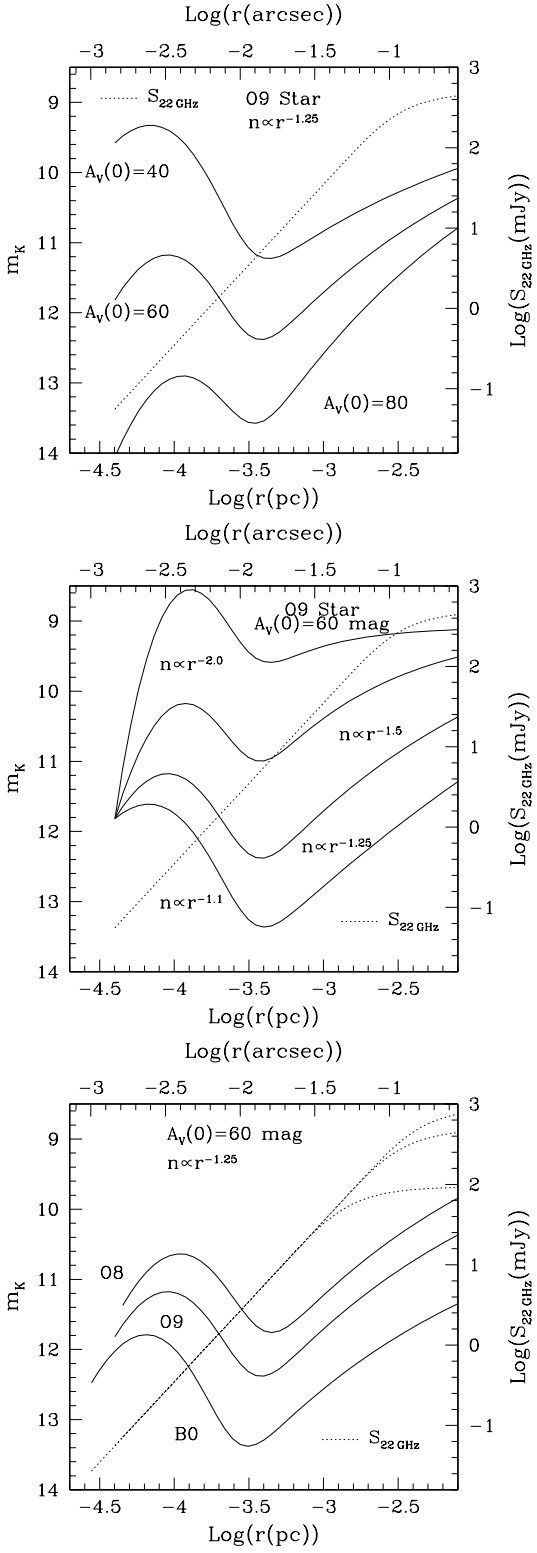

Fig. 5. Dependence of the K-band and 22 GHz emission on the three main parameters of the model: $A_V(0)$ (top panel), the index of the density power-law (central panel) and the spectral type of the ionizing star (lower panel). In all plots the K-band emission is presented as a solid line (the scale is that on the left axis), and the 22 GHz flux is presented as a dotted line (the scale is that on the right axis). The models have been calculated assuming a distance of 5.7 kpc.

be surrounded by a hot dust envelope, with the dust as close to the star as permitted by the sublimation temperature. As the HII region expands, the dust close to the star will be destroyed by the ionizing radiation and pushed outward by the radiation pressure and the stellar wind. Thus, as the time increases and the UC HII region expands, we expect the temperature of the dust that emits in the near infrared to drop approximately as $r^{-1/2}$, where r is the radius of the UC HII region. The effective increase in the emitting surface (as r^2) of the hot dust shell does not balance the decrease in its temperature (due to the exponential dependence on T in the Wien region of the black-body spectrum), and the NIR dust emission drops rapidly with r.

On the other hand, the cm radio continuum emission of the ionized gas will be optically thick and self-absorbed in the first

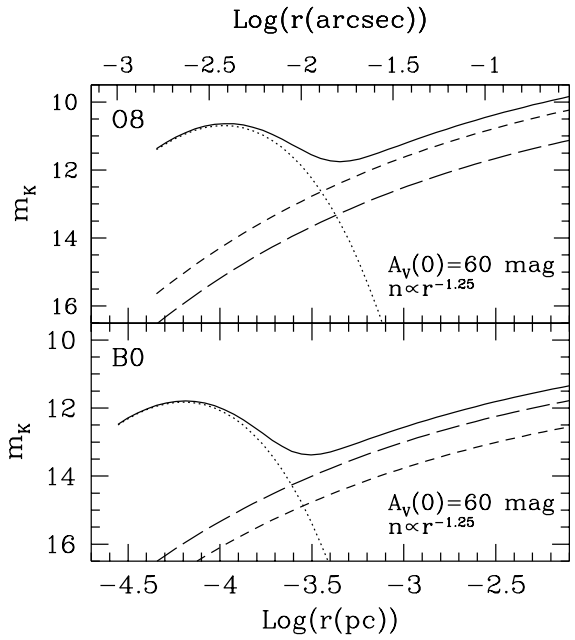

Fig. 6. K-band emission of the three components of the model, for an O8 (upper panel) and a B0 (lower panel) ZAMS star. The solid line represents the total emission, the dotted line the "hot layer", the short dashed line the continuum emission of the ionized gas, and the long dashed line the contribution of the stellar photosphere.

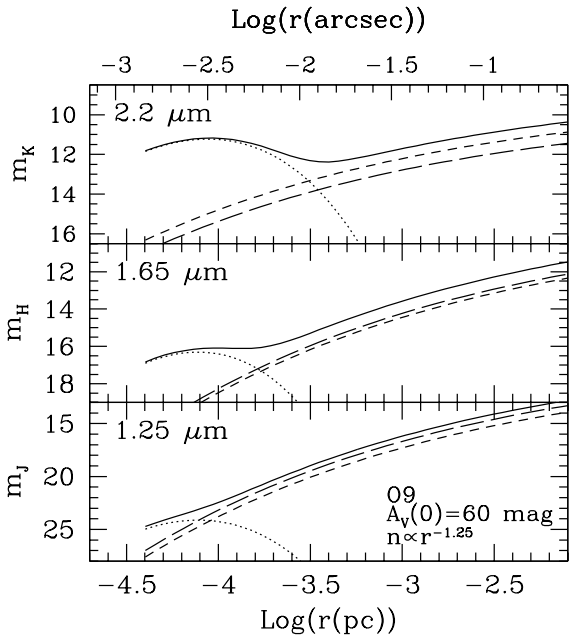

Fig. 7. K-band (upper panel), H-band (central panel) and J-band (lower panel) emission of the three components of the model, for an O9 ZAMS star. The three different components are represented as in Fig. 6.

stages, when the radius of the HII region, r, is small. At a given frequency, as r increases, the radio continuum emission of the HII region increases (until eventually becomes optically thin) making the ionized gas detectable.

To develop a simple model, we assume that the ionized region is spherical and the density is uniform within the HII region at any time, but variable with the radius r of the HII region (which in turn depends on the *age* of the source) in a way to always balance the ionizing stellar radiation, which is kept constant. The hot dust is present only outside the HII region and it emits like a black body at temperature $T(r)$ defined by the thermal balance with the stellar radiation field. The external cooler parts of the envelope provide only the extinction in the NIR, and emit the bulk of the far infrared and submillimeter radiation with negligible contribution in the NIR. The extinction is computed assuming a power law density distribution in the neutral part of the clump and a radius of the clump R = 0.5 pc. Hence it has a maximum at the beginning and decreases as r increases. In the calculation we parametrize A_V (the equivalent extinction in the V band) in terms of $A_V(0)$, the extinction at the beginning of the simulation, and the power law index of the density distribution. For all the model simulations we have assumed a distance of 5.7 kpc.

Under these assumptions the K-band emission and the free-free radio continuum emission (for instance at 22 GHz) depend only on the assumed spectral type of the central star, the extinction provided by the cool dust, and the radius of the ionized region.

In Fig. 5 the observed magnitude at K and the radio continuum flux at 22 GHz are presented as a function of the radius of the ionized region. In the three panels the dependence of the K-band and 22 GHz continuum on the three main parameters of the model is shown. In the upper panel of Fig. 5 three different simulations for an O9 zero age main sequence (ZAMS) star and a density profile $n \propto r^{-1.25}$ are given for $A_V(0)$ = 40, 60 and 80 mag. The cm radio continuum emission, which, under our assumptions, depends only on the number of ionizing photons available, is the same in all the three models and depends only on the size of the HII region. The K-band emission is dominated by the "hot dust layer" for $r \lesssim 5 \times 10^{-4}$ pc, then there is a minimum in the emission for increasing r when the dust becomes too cold to emit significantly at 2.2 μm and the stellar and the free-free and free-bound emission from the ionized gas are still too extincted. Finally, the emission rises again as the extinction decreases. In practice the hot dust produces a peak of K-band emission at small radii in spite of the high extinction; then there is a minimum in the K emission due to the drop of the "hot dust layer" temperature; while at large radii the contribution of the star and ionized gas raises the K emission again when the extinction drops.

In the central panel of Fig. 5 we present four simulations for an O9 ZAMS star, $A_V(0)$ = 60 mag and for density profiles with power law indices 1.1, 1.25, 1.50, and 2.0. The qualitative behaviour of the models is very similar to that of the previous models.

In the lower panel of Fig. 5 three simulations for $A_V(0)$ = 60 mag, $n \propto r^{-1.25}$ and different spectral types B0, O9 and O8

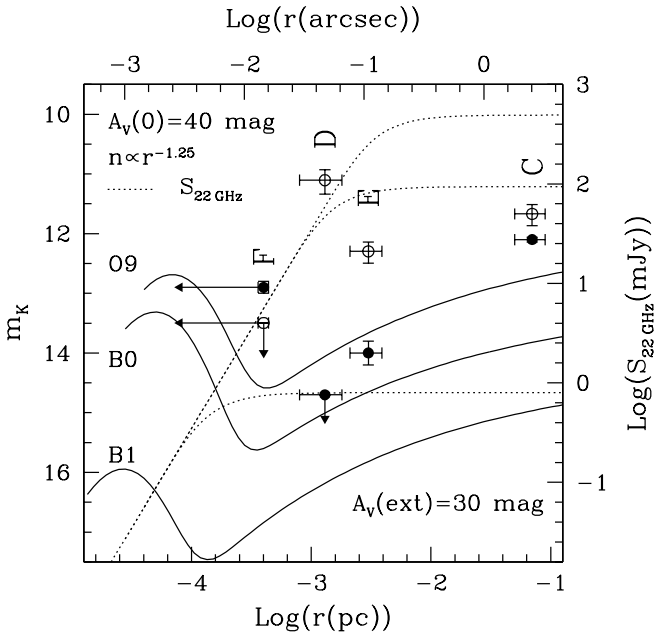

Fig. 8. Infrared K-band and radio continuum observations of components C, D, E, and F are compared with the predictions of some models. Open symbols represent the radio continuum emission measured at 22 GHz by CCHWK (note that for component F we report an upper limit of 1 mJy). Filled symbols represent our infrared measurements (see Table 1). Upper limits are indicated with arrows. We use the sizes of sources C and E reported by CCHWK (note that we use the *radius*). An external ambient extinction of A_V =30 mag has been added.

ZAMS stars are presented. Also in these cases the qualitative behaviours of the curves are similar to the previous simulations.

The general trend shown by all the simulations is that when r is small (say less than 100 AU), i.e. when the region is very young, the near infrared emission is high due to the hot dust near the stellar photosphere, while the radio continuum emission is strongly self absorbed. As the radius increases (i.e. at later times) the NIR emission drops and the radio emission rises toward the optically thin value. At large radii ($r \gtrsim 10^{-3}$ pc) only the star and the free-free and free-bound radiation from the ionized gas contribute to the emission at K, which increases as the extinction decreases due to the erosion of the inner part of the molecular cloud by the expanding HII region. The "height" of the peak of the K emission at small radii (i.e. the difference in magnitudes between the peak and the minimum in the emission at $\log(r) \simeq -3.5$ pc) depends on the model parameters, but, in the range of parameters that we have explored, is between 1 and 2 magnitudes.

In Fig. 6 the contributions of the three emissions at K-band are shown for two different central stars (O8 and B0 ZAMS). Note that the contribution of the free-free and free-bound emission from the ionized gas is smaller than the contribution of the stellar photosphere for a B0 ZAMS star, whereas the opposite holds for an O8 ZAMS star. In Fig. 7 the three contributions at J, H and K band are shown for an O9 ZAMS star. The "hot layer" of dust in the surrounding envelope dominates the infrared emission at small radii only in the K and H bands; at J the dust emission is always very low and the source should not be detectable in the early stages of evolution.

This model may explain, at least qualitatively, the differences observed between sources D, E, and F. In fact, source F is probably in the stage of very small r, when the radio continuum emission is below the mJy level, and the K-band emission is near its peak; source D is in the phase in which: 1) the radio continuum emission has almost reached the peak, 2) the dust shell is too large and too cold to emit at NIR wavelengths and 3) the extinction too high to detect the stellar and ionized gas free-free and free-bound emission in the NIR. Source E is in the phase in which the NIR emission becomes detectable again and the radio continuum emission is optically thin. Source C is similar to E but in a more evolved stage, since it is not associated either to molecular or mm continuum emission.

In Fig. 8 our near infrared and CCHWK radio continuum measures for sources C, D, E, and F are compared with the predictions of the model. Open dots refer to the radio continuum measurements, while filled dots are the NIR measurements. An external (constant) ambient extinction of A_V = 30 mag (as measured toward source NIR-B⋆) has been added to the model. The sizes of sources C, D and E are those measured by CCHWK and Hofner et al. (1996). The upper limit on the size of source F has been derived assuming that CCHWK does not detect the source due to beam dilution (see Sect. 3.5). We positioned it on the graph at 10^{-4} pc. The agreement of the prediction of the model in the radio and NIR bands and the observations is generally rather good, considering the crudeness of the model.

It is worth pointing out some obvious limitations of our model and the proper range in which it can be used: 1) at very small radii ($r \lesssim 6 \times 10^{-5}$ pc) the near infrared emission decrease is due to the higher values of the extinction in the first stages of the simulations. Clearly, a full radiative transfer calculation should be performed at small radii. 2) other processes not taken into account in this simple model may contribute to the NIR emission, such as the hot dust inside the HII region, an accretion disk close to the star and line emission. 3) finally, most of the sources observed in detail show non-spherical geometries. For example in W75N (Moore et al. 1991; Hunter et al. 1994) and in IRAS20126+4104 (Cesaroni et al. 1997) the NIR morphology of the source is highly asymmetric and there are clear indications that most of the infrared radiation is actually starlight plus circumstellar emission reflected in large scale lobes. However, these cases can be clearly distinguished from source F since the NIR emission does *not* coincide with the molecular and mm-continuum peak.

4.2. The maser activity

In the Medicina single dish observations, the water maser is variable (as in almost all known star formation H_2O masers) but not as much as observed in other sources as for instance W75N (Hunter et al. 1994) and S235B (Felli et al. 1997). From the limited data that we have, we can see that the shape of the spectrum does not change much during the years, and the

components between 0 and 10 km/s have raised their intensity by a factor of two in 8 years.

The fact that the masers are associated with the earliest evolutionary phases of a YSO fits nicely with the qualitative model described above. In fact, the maser sources are expected to be pumped efficiently only close to the YSO, between 10^{14} cm and 10^{16} cm. This corrensponds exactly to the region close to the K-band peak due to the hot shell NIR emission. YSOs equally bright at K but with a more extended UCHII region (i.e. with the NIR emission coming from stellar and ionized gas contributions) do not show associated H_2O maser emission.

5. Conclusions

In this paper we have presented new NIR observations in the J, H and K broad bands of the G9.62+0.19 star forming region. The NIR observations have been compared with published high resolution radio continuum and molecular line observations in the centimetric and millimetric bands.

The infrared observations enabled us to the detect the photospheric emission of the ionizing stars associated with the more evolved UC HII regions as well as the *free-free* and *free-bound* emission from the ionized gas (components E, C, and B). The most compact (and presumably younger) of the UC HII regions (component D) has not been detected at NIR wavelengths. The mm-continuum and molecular component F (which is not associated to any detected centimetric radio continuum emission) has been detected at K-band.

We propose a simple evolutionary model which is able to explain the infrared and radio morphology of the young massive stars in the complex. A young massive star is surrounded by a spherical ionized region and a dusty envelope, as the HII region expands the envelope is eroded. In the near infrared the emission is produced by: 1) the stellar photosphere, 2) the *free-free* and *free-bound* radiation from the ionized gas and 3) the hottest layer of the dusty envelope. The cooler parts of the envelope provide the extinction. When the source is young and the HII region is compact and self-absorbed, the dusty envelope is close to the star and the dust, heated by the stellar radiation, emits strongly in the K band. In spite of the high value of the extinction in these early phases, the hot dust emission is observable at K, while the cm radio continuum from the HII region is too self-absorbed to be detectable (component F is expected to be in this evolutionary phase). As the HII region expands the radio *free-free* emission becomes detectable, but the dust cools down rapidly and the K-band emission drops since the star and ionized gas are still too extincted to be detectable (component D). The K-band emission rises again, due to the contributions of the stellar photosphere and *free-free* and *free-bound* radiation from the ionized gas, when the exctinction drops due to the erosion of the molecular cloud by the UC HII region.

In this picture the H_2O maser activity is associated with the earliest evolutionary phases, in which the ionized gas is confined in a sub-milliparsec region around the young star.

Acknowledgements. We thank Riccardo Cesaroni for providing the VLA maps of CCHWK and for carefully reading the manuscript. Support from C.N.R.–N.A.T.O. Advanced Fellowship program and from NASA's *Origins of Solar Systems* program (through grant NAGW–4030) is gratefully aknowledged.

References

Beckwith S., Sargent A.I., Chini R.S., Güsten R., 1990, AJ, 99, 924
Brand J., et al. 1994, A&AS, 103, 541
Calvet N., Hartmann L. & Strom S.E., 1997, ApJ, 481, 912
Casali M., & Hawardeen T., 1992, JCMT-UKIRT Newsletter, No. 4, p. 33
Cesaroni R., Walmsley C.M., Kömpe C., Churchwell E., 1991, A&A, 252, 278
Cesaroni R., Walmsley C.M., Churchwell E., 1992, A&A, 256, 618
Cesaroni R., Churchwell E., Hofner P., Walmsley C.M., Kurtz S., 1994, A&A, 288, 903, CCHWK
Cesaroni R., Felli M., Testi L., Walmsley C.M., Olmi L., 1997, A&A, in press
Churchwell E., Wolfire M.G., Wood D.O.S., 1990, ApJ, 354, 247
Codella C., Felli M., Natale V., Palagi F., Palla F., 1994, A&A, 291, 261
Codella C., Testi L., Cesaroni R., 1997, A&A, in press
Felli M., Testi L., Valdettaro R., Wang J.-J., 1997, A&A, 320, 594
Forster J.R. 1993, in "*Astrophysical Masers*", eds. A.W. Clegg & G.E. Nedoluha (Heidelberg, Springer), p. 108
Forster J.R., & Caswell J.L., 1989, A&A, 213, 339
Garay G., Rodeiguez L.F., Moran J.M., Churchwell E., 1993, ApJ, 418,368
Hofner P., & Churchwell E., 1996, A&AS, 120, 283
Hofner P., Kurtz S., Churchwell E., Walmsley C.M., Cesaroni R., 1994, ApJ, 429, L85
Hofner P., Kurtz S., Churchwell E., Walmsley C.M., Cesaroni R., 1996, ApJ, 460, 359
Hunt L.K., Testi L., Borelli S., Maiolino R., Moriondo G., 1994, Technical Report 4/94, Arcetri Astrophysical Observatory
Hunter T.R., Taylor G.B., Felli M., Tofani G., 1994, A&A, 284, 215
Hunter T.R., Testi L., Taylor G.B., Tofani G., Felli M., Phillips T.G., 1995, A&A, 302, 249
Jenness T., et al., 1996, MNRAS, 276, 1024
Koornneef J., 1983, A&A, 128, 84
Kurtz S., Churchwell E., Wood D.O.S., 1994, ApJS, 91, 659
Moore T.J.T., Mountain C.M., Yamashita T., McLean I.S., 1991, MNRAS, 248, 377
Natta A., Palla F., Butner H.M., Evans N.J.II, Harvey P.M., 1993, ApJ, 406, 674
Natta A. & Panagia N., 1976, A&A, 50, 191
Norris R.P., Whiteoak J.B., Caswell J.L., Wieringa M.H., Gough R.G., 1993, ApJ, 412, 222
Palla F., Cesaroni R., Brand J., Caselli P., Comoretto G., Felli M., 1993, A&A, 280, 509
Palla F., Testi L., Hunter T.R., Taylor G.B., Prusti T., Felli M., Natta A., Stanga R.M., 1995, A&A, 293, 521
Persi P., Felli M., Lagage P.O., Roth M., Testi L., 1997, A&A, in press
Persi P., Roth M., Tapia M., Marenzi A.R., Felli M., Testi L., Ferrari–Toniolo M., 1996, A&A, 307, 591
Persson S.E. West S.C., Carr D.M., Sivaramakrishnan A., Murphy D.C., 1992, PASP, 104, 204
Rieke G.H. & Lebofsky M.J., 1985, ApJ, 288, 618
Sibille F., Lunel M., Bergeat J., 1974, Astr. and Space Science, 30, 173
Schmidt-Kaler Th. 1981, in Landolt-Börnstein, Gruppe VI, Bond 2, 1 (publ. Springer)

Testi L., 1993, Technical Report 10/93, Arcetri Astrophysical Observatory
Testi L., Felli M., Persi P., Roth M., 1994, A&A, 288, 634
Testi L., Felli M., Persi P., 1995, Mem. S. A. It., v. 66, p. 677
Testi L., Felli M., Persi P., Roth M., 1997, A&AS, submitted
Tofani G., Felli M., Taylor G.B., Hunter T.R. 1995, A&AS, 112, 299
Walmsley C.M. 1995, RevMexAA SC, 1, 137

This article was processed by the author using Springer-Verlag LaTeX
A&A style file *L-AA* version 3.